Bull Earthquake Eng (2015) 13:3107–3133
DOI 10.1007/s10518-015-9746-x

ORIGINAL RESEARCH PAPER

Seismic behavior of three-leaf stone masonry buildings before and after interventions: Shaking table tests on a two-storey masonry model

Elizabeth Vintzileou[1] · Charalambos Mouzakis[2] · Chrissy-Elpida Adami[1] · Lucia Karapitta[2]

Received: 14 May 2014 / Accepted: 11 March 2015 / Published online: 5 April 2015

Abstract The aim of this work is to reach a better understanding of the seismic behaviour of historic three-leaf stone masonry buildings with timber floors, before and after interventions. For this purpose, shaking table tests were performed on a building model (scale 1:2). Initially, the dynamic characteristics of the model were identified. Subsequently, biaxial earthquake tests were performed with the base acceleration increased step-wise until the occurrence of repairable damages. Afterwards, the masonry was strengthened by means of grouting and the diaphragm action of the floors was enhanced. Then, the strengthened model was re-tested. The comparison of the performance of the model under earthquake actions before and after strengthening shows that the selected intervention techniques significantly improved the seismic behaviour of the structure.

Keywords Diaphragm action · Grout injection · Seismic behaviour · Shaking table tests · Three-leaf stone masonry

1 Introduction

Stone masonry, used in Europe and elsewhere for the construction of historic buildings, is a general term covering several typologies (dry construction or stones laid in mortar, single-, double- or three-leaf masonry). Three-leaf stone masonry, frequently met in historic

✉ Charalambos Mouzakis
harrismo@central.ntua.gr

✉ Chrissy-Elpida Adami
adamis@central.ntua.gr

[1] Faculty of Civil Engineering, Laboratory of Reinforced Concrete, National Technical University of Athens, 9 Iroon Polytechniou str., 15773 Athens, Greece

[2] Faculty of Civil Engineering, Laboratory for Earthquake Engineering, National Technical University of Athens, 9 Iroon Polytechniou str., 15773 Athens, Greece

buildings, is made of two exterior leaves with the space between them filled with poor quality material (pieces of stones and/or bricks and mortar). Three-leaf masonry is one of the most vulnerable types of masonry. On the other hand, historic buildings are typically provided with timber floors and roofs. Due to the insufficient in-plane stiffness of those timber diaphragms Tomaževic (1992), Tomaževic et al. (1993), Giuffrè et al. (1993), Giuffrè and Carrocci (1999), FEMA 356 2000, ASCE 41-06 2007, Oliver (2010), Wilson (2012), as well as due to their inadequate connection with vertical bearing elements, walls are not subject to equal displacements during seismic events. The result of those structural characteristics is the pronounced seismic vulnerability of old masonry buildings.

Indeed, past and recent earthquakes have caused severe damages to cultural heritage assets (see i.a. http://www.eeri.org/site/projects/learning-from-earthquakes; Giuffrè et al. 1993; Giuffrè and Carrocci 1999). Thus, the need was felt by the international scientific community to investigate the mechanical behaviour of stone masonry buildings on the basis of tests at material and at element level, as well as on subassemblies and on building models. Part of this research is devoted to the investigation of three-leaf stone masonry structures: (a) Masonry wallettes were tested under static actions in compression and/or in diagonal compression to assess basic mechanical properties of masonry at its as-built state. Moreover, in order to evaluate the effect of various intervention techniques on the mechanical properties of three-leaf masonry, wallettes were tested, for example, after the application of grouting and transversal steel ties. Grouting was efficient in enhancing the mechanical properties of the filling material, whereas both investigated techniques have improved the bond between masonry leaves, thus preventing their premature separation (see i.a. Toumbakari 2002; Toumbakari et al. 2003; Valluzzi et al. 2001; Vintzileou and Tassios 1995; Vintzileou 2011; Binda et al. 1993; Miltiadou-Fezans et al. 2006; Adami et al. 2012). (b) Three-leaf stone masonry walls under cyclic in- or out-of-plane actions were tested in a limited number of experimental campaigns; Tomaževic and Sheppard (1982), Mazzon (2010) and Vasconcelos and Lourenco (2009) investigated the in-plane behaviour of walls, whereas Manoledaki et al. (2012) and Valluzzi et al. (2013) studied the out-of-plane response through quasi-static and dynamic tests, respectively. (c) Although several building models made of two-leaf stone masonry were subjected to dynamic loading (see i.a. Gavrilovic et al. 1987-cited by Shendova et al. 2012; Tomaževic 1992; Tomaževic et al. 1993; Benedetti et al. 1998; Juhasova et al. 2008; Meguro et al. 2012; Magenes et al. 2010, 2012a, b), the respective data on three-leaf stone masonry building models are still very limited. Recently, Mazzon et al. (2009), in his tests on scaled two-storey three-leaf stone masonry building models has observed that the governing failure mechanism of walls subjected to out-of-plane bending was due to the early separation of the leaves. Hydraulic lime based grouts applied to the walls have prevented the separation of masonry leaves and, by way of consequence, they have led to significant enhancement of the seismic resistance of the models. Significant typical characteristics of historic masonry buildings, such as inadequate wall-to-wall and wall-to-floor connections, as well as the in-plane deformability of timber floors, were experimentally investigated by Tomaževic et al. (1993), Benedetti et al. (1998) and more recently by Magenes et al. (2010, 2012a, b) on two-leaf stone masonry building models. In those studies, the negative effect of insufficient diaphragm action of flexible wooden floors on the seismic response of buildings was alleviated by applying several intervention techniques [e.g. horizontal prestressed (Tomaževic et al. 1993) or non-prestressed tendons at the level of floors (Tomaževic et al. 1993; Benedetti et al. 1998), steel grids nailed to slabs and covered by a cement mortar layer (Benedetti et al. 1998), double planking/connection with wall, replacement of floors with brick vault (Tomaževic et al. 1993) or RC slabs (Tomaževic et al.

1993; Magenes et al. 2012b)]. It should be noted that, in case of RC slabs (replacing original timber floors), concentration of cracks (Magenes et al. 2012b) and severe crushing (Tomaževic et al. 1993) at the corners of the models due to rocking mechanism was observed. Moreover, Magenes et al. (2012b) suggest that the enhancement of the seismic performance of stone masonry buildings relates more to the improvement of the roof or floor-to- wall connection, than to a high in-plane stiffness of the floors.

In the study presented herein, shaking table tests were performed with the aim to reach a better understanding of the seismic behaviour of historic three-leaf stone masonry buildings with timber floors. Furthermore, a scheme of intervention techniques was adopted, comprising (a) grouting of walls using a hydraulic lime based grout, (b) enhancement of the diaphragm action of floors and (c) connection between diaphragms and bearing walls. Grouting resulted to an increase of the bearing capacity of masonry walls in shear and in out-of-plane bending, as well as to a modification of the sequence of their failure mechanisms. The stiffening of the floors and their connections to the walls led to significant improvement of the overall response of the structure, more specifically, to substantial reduction of the out-of-plane deformations of masonry walls.

2 Experimental programme: plain masonry building model

A two-storey plain three-leaf stone masonry model (Plain Building Model-PBM) of a traditional building was built at a reduced scale of 1:2. The building model (Plain Building Model-Before Strengthening-PBM-BS) shown in Fig. 1, was subjected to seismic excitations at the facility of the Laboratory for Earthquake Engineering/National Technical University of Athens (LEE/NTUA). It should be mentioned that some minor cracks appeared on the as-built specimen before the execution of the shaking table tests. The dynamic characteristics of the specimen were first measured. Subsequently, biaxial earthquake tests were performed with the base acceleration increasing stepwise. Thus, the gradual occurrence of damages could be recorded. The experimental campaign of the as-built model continued until the occurrence of significant, but repairable damages.

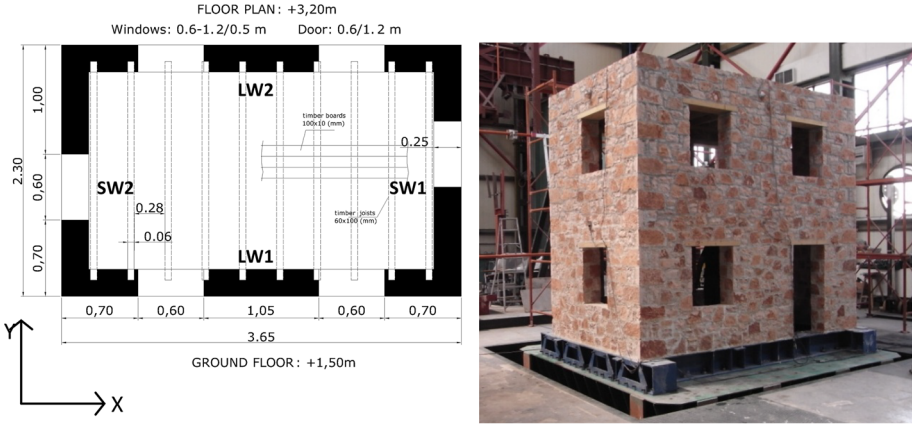

Fig. 1 **a** Typical plan of the tested building model; **b** the model on the shaking table

Afterwards, the building was repaired and strengthened (a) by means of grouting of the three-leaf masonry walls using a natural hydraulic lime based grout, (b) by enhancing the diaphragm action of the timber floors and (c) by connecting the floors to the walls. Thereafter, the Plain Building Model-After Strengthening (PBM-AS) was re-tested until large deformations and extensive damage occurred. It is noted that the tested model respected the dynamic similitude laws proposed by Harris and Sabnis (1999). However, the selected seismic inputs were not time-scaled. As a consequence, the results of this study may not be directly extrapolated to real scale structures.

2.1 Geometry of PBM

As shown in Fig. 1, a non-symmetric plan of a building was selected: the dimension of the typical floor is 3.65 × 2.30 m^2. The height of each floor is equal to 1.60 m, whereas the total height of the specimen equals to 3.20 m. The walls are 0.25 m thick. Due to the selected geometry, some walls of the model are slender, while other walls are squat.

2.2 Construction details-materials

2.2.1 Masonry

The walls of PBM were made of three-leaf stone masonry. The three leaves were of approximately equal thickness. At the four corners of the specimen, quoins were placed crosswise throughout the height of the model (see Fig. 2) to provide good connection between longitudinal and transverse walls, as it is the case in real structures. For the construction of the exterior and interior leaves of the walls, limestone units and mortar was used. The mean compressive strength and the density of the limestone are approximately equal to 100 MPa and 2.68 Mgr/m^3 respectively. For the mortar, lime putty, pozzolan and an aggregate mix composed of silicate and limestone were used. The mix proportions of the mortar, as well as its main physical and mechanical properties, are given in Table 1. The thickness of both bed and vertical joints was approximately equal to 10 mm. The intermediate part of the walls (see Fig. 2) consists of pieces of stones and mortar in a proportion of 2/1. In order to simulate the characteristics of filling material in real

Fig. 2 Construction details of the walls

Table 1 Composition and mechanical properties of mortar (determined according to EN196:1:1994)

Composition (wt%)			Water (wt% of cementitious solids)	Mechanical properties			ρ (Mgr/m^3)
Lime putty	Pozzolan	Aggregates		Age (days)	$f_{m,c}$ (MPa)	$f_{m,fl}$ (MPa)	
20	20	60	50	28	3.50	0.70	1.73
				90	4.60	0.60	1.76

$f_{m,c}$ and $f_{m,fl}$ denote the mean compressive strength and flexural strength of the mortar respectively

structures, the aim was to reach a percentage of voids of approximately 40 %. Thus, the mix of stones and mortar was placed without any compaction in the space between the exterior stone leaves. No header stones were provided for the transverse connection of the exterior leaves of masonry. To avoid the formation of cracks due to drying shrinkage, the model was cured during its construction. Actually, the moisture conditions were controlled by covering the specimen using a wet hessian cloth.

In parallel with the construction of the building model and in order to obtain data for the mechanical properties of masonry, two wallettes (of the same scale with the building model) were constructed and tested in compression. Tests were carried out according to EN 1052-1-1998. Figure 3a, b shows the setup for testing the wallettes in compression. Load-controlled tests were carried out. Deformations were measured by means of displacement transducers: Four sensors (two per wallette face) were used to measure vertical deformations; two sensors (one per wallette face) were placed to measure horizontal deformations (and vertical crack openings), while two sensors (one per side) were recording the transverse deformations of the wallettes (i.e. separation between masonry leaves).

One specimen was tested up to collapse (Wallette 1). The other wallette was tested until significant damage occurred (Wallette 2). Subsequently, it was grouted with the same hydraulic lime based grout used to the building model. Approximately 6 months after the application of grout, the strengthened wallette was re-tested to failure. In Fig. 3c, the compressive stress versus vertical strain curves are given for Wallette 1 tested as-built and

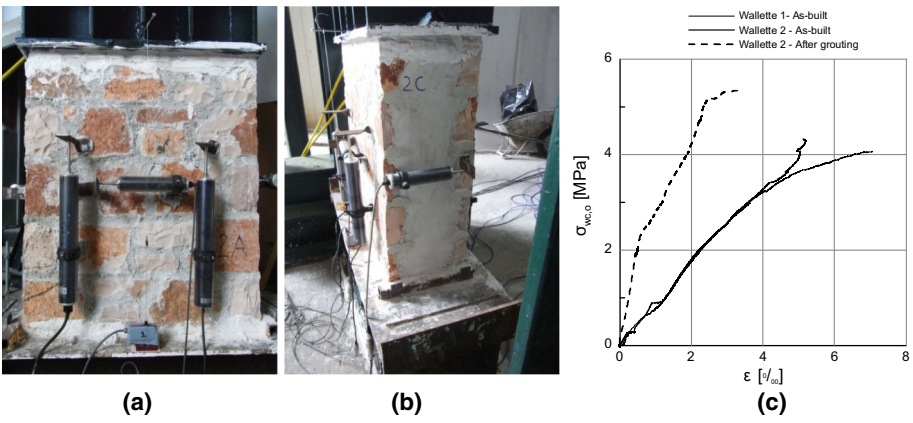

Fig. 3 Wallettes subjected to compression. **a–b** Test setup and instrumentation, **c** compressive stress versus vertical strain curves for wallettes before and after grouting

for Wallette 2 tested as built and after grouting. Table 2 summarizes the mechanical properties of the wallettes before and after grouting. One may observe that both compressive strength and stiffness of masonry were enhanced due to grouting.

2.2.2 Timber elements

Timber lintels were provided to all openings of PBM (Fig. 4a). The floors consist of timber joists (60×100 mm^2) spaced at 340 mm (Fig. 4b). They are supported by masonry through a perimeter wooden collector beam (Fig. 4c). The floors are paved using 100×10 mm^2 timber boards laid perpendicular to the floor joists and nailed to them (two nails per joist, see Fig. 4d). All timber elements belong to strength class C22 (according to EN 338-2003). It should be noted that the timber joists are supported by the long walls of the model. On the basis of their geometry, the floors are classified as flexible (ASCE 41-06 2007).

It should also be mentioned that, due to the fact that the floor rests through the wooden collector beam on the interior leaf of the three-leaf masonry (see Fig. 4b, c), the vertical loads acting on the floors (self weight of the floors and additional masses) are transferred eccentrically to the vertical elements, with the interior leaf being subjected to higher vertical stresses than the exterior one.

2.2.3 Repair/strengthening techniques

After the completion of the as-built model (PBM-BS) testing, the specimen was strengthened. Masonry was grouted, whereas the existing diaphragms were stiffened and tied to masonry walls.

For the grouting of masonry, a natural hydraulic lime based grout was used. The mix proportions were: 90 % pure NHL5 and 10 % superfine natural pozzolan, commercially available as μ-silica, W type (Badogiannis et al. 2012). Table 3 summarizes the

Table 2 Mechanical properties of wallettes before and after grouting

Wallete	$f_{wc,o}$ (MPa)	$f_{wc,j}$ (MPa)	$f_{wc,j}/f_{wc,o}$	$E_{wc,o}$ (GPa)	$E_{wc,j}$ (GPa)	$E_{wc,j}/E_{wc,o}$
1-initial	4.33	–	–	0.84	–	–
2-initial/2-grouted	4.07	5.45	1.33	0.88	3.34	4.35

$f_{wc,o}$ and $E_{wc,o}$ denote the compressive strength and the modulus of elasticity of the wallettes at their original state, $f_{wc,j}$ and $E_{wc,j}$ denote the compressive strength and the modulus of elasticity of the wallettes after grouting

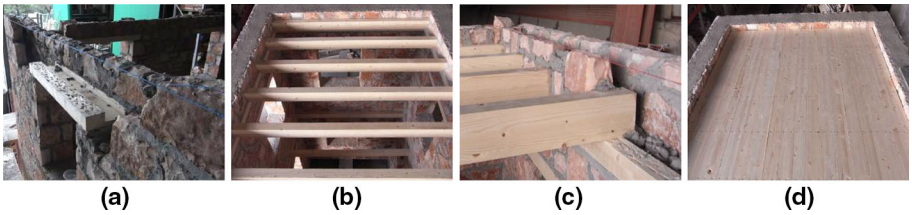

Fig. 4 Structural details of the timber elements of PBM. **a** Timber lintels, **b** timber joists, **c** timber joists to wooden collector beam connection, **d** timber pavement

Table 3 Mix proportions and mechanical characteristics of grouts

Composition (wt%)		SP (wt% of solids)	Water (wt% of solids)	Mechanical properties		
Solids				Age (days)	$f_{gr,c}$ (MPa)	$f_{gr,fl}$ (MPa)
NHL5 St. Astier	W-type S&B pozzolan					
90	10	0.70	82.5	28	1.70	0.60
				90	2.90	0.60

$f_{gr,c}$ and $f_{gr,fl}$ denote the mean compressive and the mean flexural strength of the grout respectively

mechanical properties of the grout. The mix to be injected to masonry was prepared using an ultrasound dispersion mixer assisted by a mechanical device of low turbulence. The mix was applied to the masonry following the procedure adopted by the Hellenic Ministry of Culture (Miltiadou-Fezans et al. 2005). Figure 5 shows pictures taken during the application of the grouting technique. In-laboratory and in situ tests (according to Miltiadou and Tassios 2012, 2013a, b) were performed to check and reach the desired properties of the grout in situ. During injection, the consumed quantity of grout was recorded. The total volume of the grout injected in the damaged as-built model was equal to 955 l. This consumption shows that the percentage of voids of the filling material was approximately equal to 32 %. This value is considered to be quite close to the target one (approx. 40 %), as well as to the percentage of voids in real three-leaf masonry.

To enhance the stiffness of wooden floors, a second pavement was placed—on top of the existing one—with the boards at an angle of 45° with respect to the original ones (ASCE 41-06 2007; Valluzzi et al. 2010). The new pavement was connected through the original one to the timber joists, using nails (Fig. 6b). The stiffened floors were connected to the perimeter walls, through a 100 × 100 × 5 m^3 steel (yield strength S235) bearing plate (placed against the exterior face of masonry) and a L80/80/8 steel element 200 mm long (placed against the interior face of masonry and bolted onto the timber floor). The two steel elements (Figs. 6a, 7), were connected using 10 mm bolts through holes drilled in masonry. The wall-to-stiffened floor connection was designed to resist a shear force three times as high as the maximum one recorded on the as-built model during its testing. As

Fig. 5 **a–b** Grouting of three-leaf masonry walls

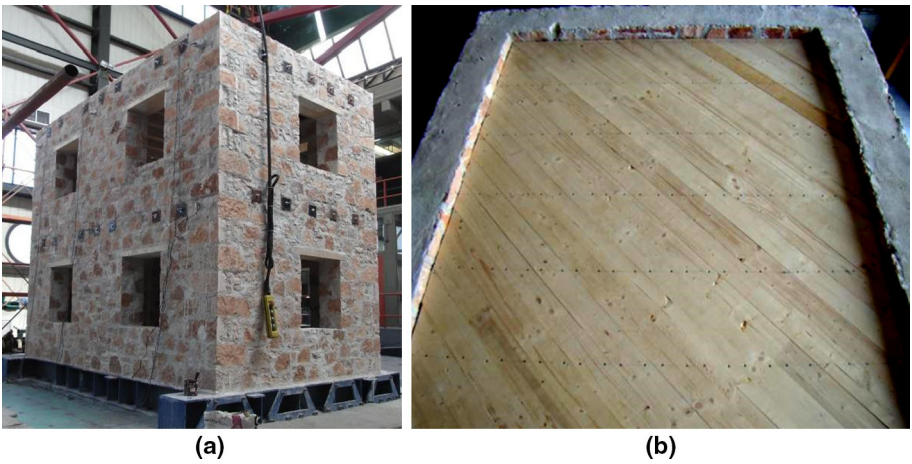

Fig. 6 Strengthened model PBM **a** general view and **b** view from the top

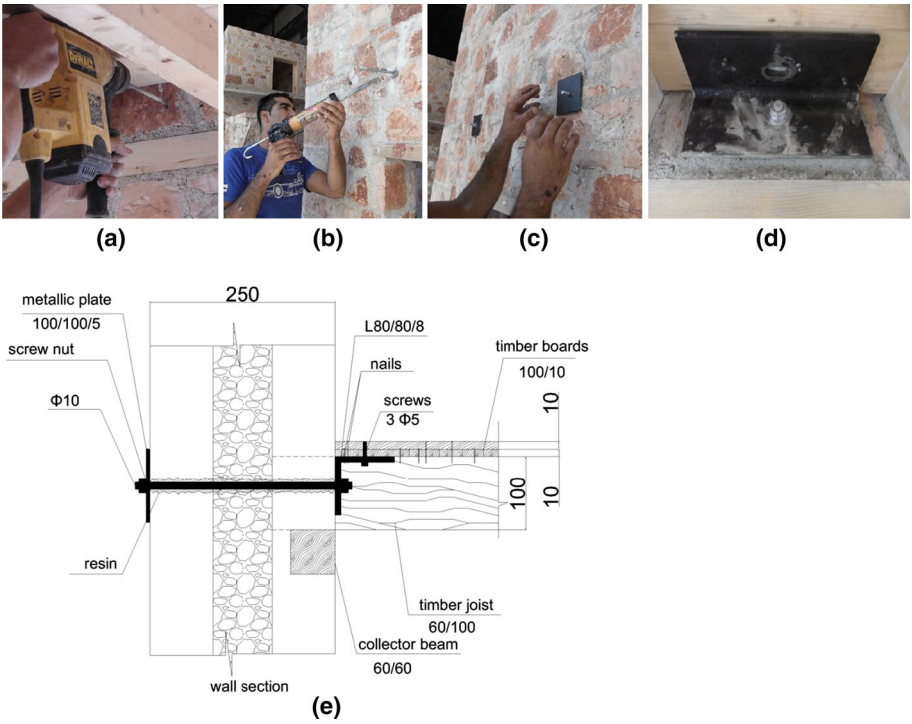

Fig. 7 Construction details of the wall to timber floor connection. **a** Drilling the wall at floor level, **b** installing the chemical bolts, **c–d** placing the steel elements at both sides of the walls, **e** wall-to-timber floor connection (drawing)

shown in Fig. 6a, long walls were connected to the floors at seven locations, whereas five anchors were used to connect the floors to the short walls.

2.2.3.1 Test-setup and instrumentation The building model was constructed on a steel base (Fig. 1b). To prevent sliding of the model, deformed steel reinforcing bars were welded on the steel base at intervals, along two orthogonal directions. Thus, mechanical interlock was ensured between the base and the first layer of mortar and stones. The adopted solution proved to be efficient, since no relative displacement between the base of the model and the steel base was observed. Before testing, the steel base was securely fastened (bolted) on the shaking table.

The instrumentation of the model is shown in Fig. 8: Sixteen (16) accelerometers and twelve (12) displacements transducers were used to measure accelerations and absolute displacements along X and Y directions at both levels. The same basic set-up was used for both testing sequences, i.e. before and after strengthening. In the case of the strengthened model, four (4) additional displacement transducers were used to measure relative floor-to-wall displacements. Such relative displacements need to be detected as they allow for the efficiency of the connection between horizontal and vertical bearing elements to be assessed. The additional displacement traducers were placed at mid-length of the floors at both storeys (i.e. D13 and D14 along Y-direction, D15-D16 along X-direction in Fig. 8).

The self weight of the as-built model was approximately equal to 14.5 Mgr. As shown in Fig. 9, additional masses (7.5 Mgr) were placed on the first and second floors, 4.5 and 3 Mgr respectively. The resulting mean compressive stress at the base of the model is equal to 2 % of the measured compressive strength of masonry along the Y direction. Along the X direction, the average compressive stress is higher (as the floors are supported by the long walls), equal to 7 % of the compressive strength of masonry. The additional masses were fixed to the floors with special connectors, to prevent any effect of the additional masses on the stiffness and the bearing capacity of the diaphragms. The total mass of the as-built specimen was approximately equal to 22.0 Mgr. After strengthening, the self

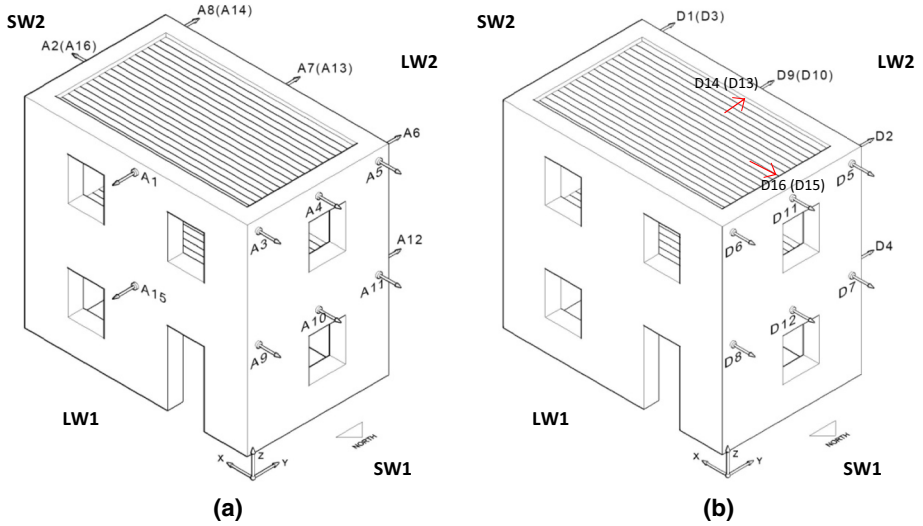

Fig. 8 Location of **a** accelerometers and **b** transducers

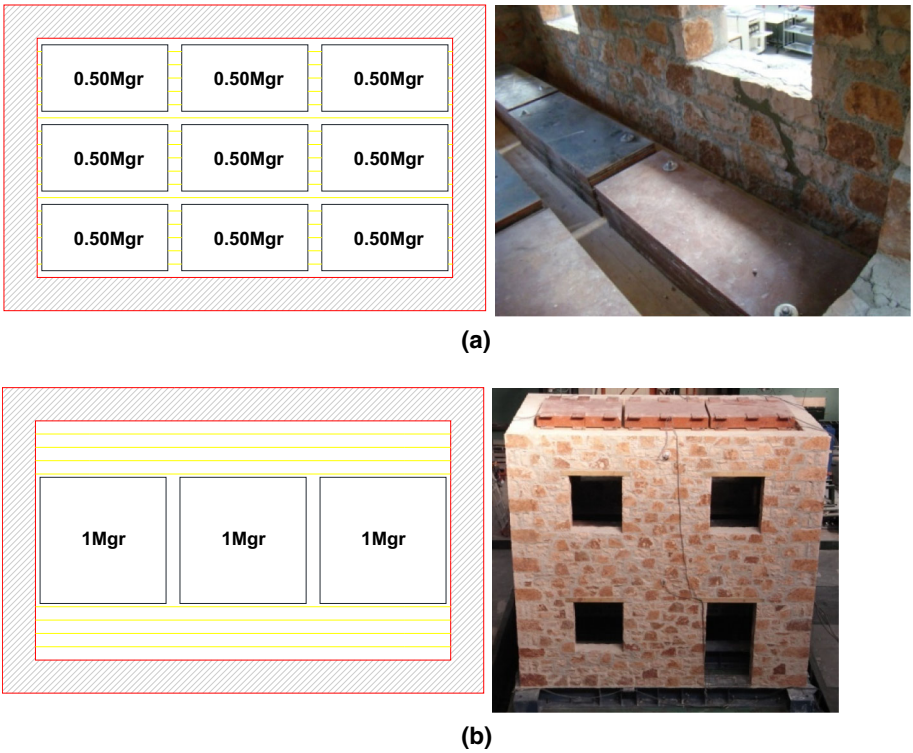

Fig. 9 Arrangement of additional masses on the floor of the **a** 1st and **b** 2nd level

weight of the model increased by 13 %. Thus, for the PBM-AS, the total mass was approximately equal to 23.5 Mgr. It should be noted that mass simulation law could not be fully respected, due to the limitations of the shaking table. Thus, the results of the tests reported in this paper cannot be directly extrapolated to the full scale structure. Such an extrapolation is being worked on, in the framework of the numerical calculations carried out by the authors.

2.2.4 Test procedure/seismic input/test protocol

PBM was tested on the shaking table under biaxial excitation along two horizontal axes. Before the application of the selected seismic inputs, the dynamic properties of the specimen were measured through low amplitude (0.02 g) sine logarithmic sweep excitation. Sine sweep tests were performed separately along X and Y direction. Subsequently, the as-built model (PBM-BS) was subjected to a series of motions with stepwise increasing maximum base acceleration, until significantly damaged. After the completion of the test, PBM was removed from the shaking table, strengthened and repositioned on the shaking table. The strengthened model (PBM-AS) was retested (subjected to a series of biaxial motions) until failure.

The as-built model (PBM-BS) was subjected to a sequence of the Kalamata signals (September 13, 1986, Ms = 6.2, max a = 0.25 g(X)/0.27 g(Y)) The test protocol is given in Table 4. The accelerogram of Kalamata earthquake was selected taking into account that

Table 4 As-built model (PBM-BS). Test protocol

No. of test	Excitation	Direction of excitation	Base acceleration (g/%)	
			X	Y
1BS	Sine sweep	X	0.02	–
2BS	Sine sweep	Y	–	0.02
3BS	Kalamata	X&Y	0.045/(18 %)	0.037/(14 %)
4BS	Kalamata	X&Y	0.10/(40 %)	0.09/(33 %)
5BS	Kalamata	X&Y	0.14/(56 %)	0.13/(48 %)
6BS[a]	Kalamata	X&Y	0.18/(72 %)	0.16/(59 %)
7BS	Kalamata	X&Y	0.22/(88 %)	0.21/(78 %)
8BS	Kalamata	X&Y	0.29/(116 %)	0.24/(89 %)

[a] Initiation of cracking

Table 5 Strengthened model (PBM-AS). Test protocol

No. of test	Excitation	Direction of excitation	Base acceleration (g/%)	
			X	Y
1AS	Sine sweep	X	0.02	–
2AS	Sine sweep	Y	–	0.02
3AS	Kalamata	X&Y	0.04/(16 %)	0.04/(15 %)
4AS	Kalamata	X&Y	0.10/(40 %)	0.09/(33 %)
5AS	Kalamata	X&Y	0.14/(56 %)	0.13/(48 %)
6AS	Kalamata	X&Y	0.19/(76 %)	0.17/(63 %)
7AS	Kalamata	X&Y	0.23/(92 %)	0.20/(74 %)
8AS	Kalamata	X&Y	0.29/(116 %)	0.25/(93 %)
9AS	Kalamata	X&Y	0.33/(132 %)	0.27/(100 %)
10AS	Kalamata	X&Y	0.40/(160 %)	0.32/(119 %)
11AS	Kalamata	X&Y	0.49/(196 %)	0.37/(137 %)
12AS	Kalamata	X&Y	0.55/(220 %)	0.39/(144 %)
13AS	Irpinia	X&Y	0.16/(123 %)	0.16/(123 %)
14AS	Irpinia	X&Y	0.34/(262 %)	0.29/(223 %)
15AS[a]	Irpinia	X&Y	0.48/(369 %)	0.43/(331 %)
16AS	Irpinia	X&Y	0.62/(477 %)	0.72/(554 %)
17AS	Irpinia	X&Y	0.54/(415 %)	0.66/(508 %)

[a] Initiation of cracking

the major spectral amplifications of motion frequencies occur in the range of frequencies of the fundamental modes of the building model in X and Y direction. The same excitation sequence was imposed to the strengthened model as well, reaching, however, higher maximum accelerations (Test 12AS: Kalamata earthquake 0.55 g(X)/0.39 g(Y), Table 5). The fact that during the Test12AS, the strengthened model (with modified dynamic characteristics) did not suffer any damage, made clear the need to proceed with another input motion, having characteristics that could lead the strengthened model to significant

damages and collapse. Thus, the first part of the Irpinia earthquake signals (November 23, 1980, Calitri record, Ms = 6.9, max a = 0.13 g(X)/0.13 g(Y)) was subsequently imposed to the strengthened model. The time histories of base accelerations for Kalamata and Irpinia signals are given in Fig. 10, whereas Fig. 11 shows the response spectra of the two motions (5 % damping).

3 Test results

Within this section, the main test results (i.e. dynamic characteristics, observed damages, maximum accelerations and relative displacements, interstorey drifts, hysteretic response, capacity curves) of the building model, tested before and after interventions, are presented and discussed upon.

3.1 Dynamic characteristics of PBM-BS and PBM-AS building model

Sine logarithmic sweep test was performed prior to the earthquake tests to determine the dynamic characteristics (natural frequencies and damping) of the model. The frequency range for the sine sweep tests was 1.0 Hz to 16 Hz along X direction and 1.0 Hz to 32 Hz along Y direction, at a rate of one octave per minute. Thus, the excitation frequency, f (in Hz), versus time, t (in s), follows the expression:

$$f = 1.00 \times 2^{t/60}$$

To prevent cracking of the model, an excitation of low amplitude (0.02 g) was selected. The frequencies were determined from the recorded acceleration at points: A2, A3, A4,

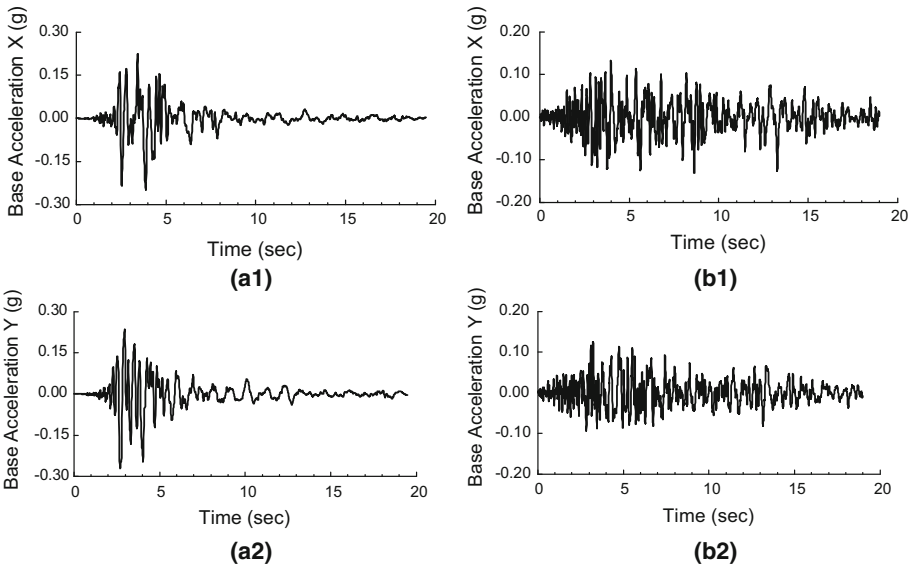

Fig. 10 Base acceleration time histories along (1) X direction and (2) Y direction for **a** Kalamata and **b** Irpinia earthquake

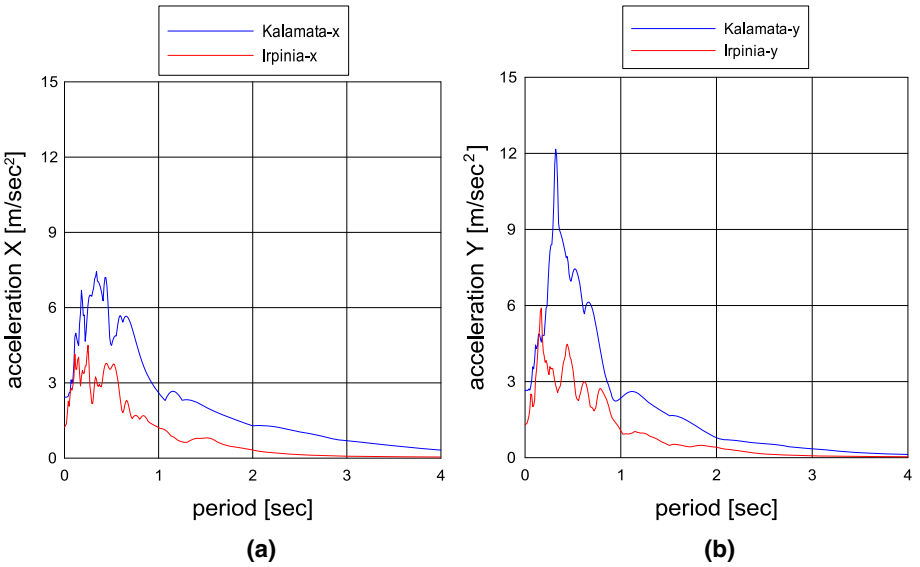

Fig. 11 Kalamata and Irpinia earthquakes. Response spectra for 5 % damping in **a** X direction and **b** Y direction

A5—for X direction and A7, A6, A8, A1—or Y direction (Fig. 8). Natural frequencies and damping ratios were calculated from the response of the tested models during sine logarithmic sweep excitations. The damping ratio was calculated using the half-power bandwidth method.

The resonance frequencies and the corresponding damping ratios at measuring points of PBM-BS and PBM-AS are shown in Fig. 12. The building model at its as-built state (PBM-BS) exhibits an average value of frequency equal to 6.05 Hz along X-direction and equal to 4.21 Hz along the Y-direction (Table 6). One may observe (Fig. 12) that there are differences in the frequencies recorded at three locations along the long walls. This feature may be attributed to the out-of-plane deformability of the long non-homogenized (though grouting) walls of the model. Actually, the difference between measured frequencies close to the corners of the model and at mid-length of the long walls is more pronounced in the upper storey. Moreover, those differences practically disappear (a) along the significantly less sensitive to out-of-plane actions short walls of PBM-BS, as well as (b) along both axes of the PBM-AS. This is attributed to the box action of the model at its strengthened state, which is significantly enhanced due to both the homogenization of masonry and the stiffening of the diaphragms, adequately connected to the walls. The damping ratio for PBM-BS is equal to 4.89 % along X direction (Table 6). Higher value of damping (6.81 %) is calculated along Y direction, due to the interaction between the timber joists of the floors and the walls.

The respective measurements for the building model after strengthening (PBM-AS) show a significant increase of the frequency, attributed to the stiffening of the model due to the applied interventions. Furthermore, almost equal values of frequency were measured along both axes of the model, as well as at all locations along each wall. Therefore, the almost perfect box behaviour of the strengthened model is evident. Along the same line, the damping ratio of the strengthened model is significantly lower than that measured on

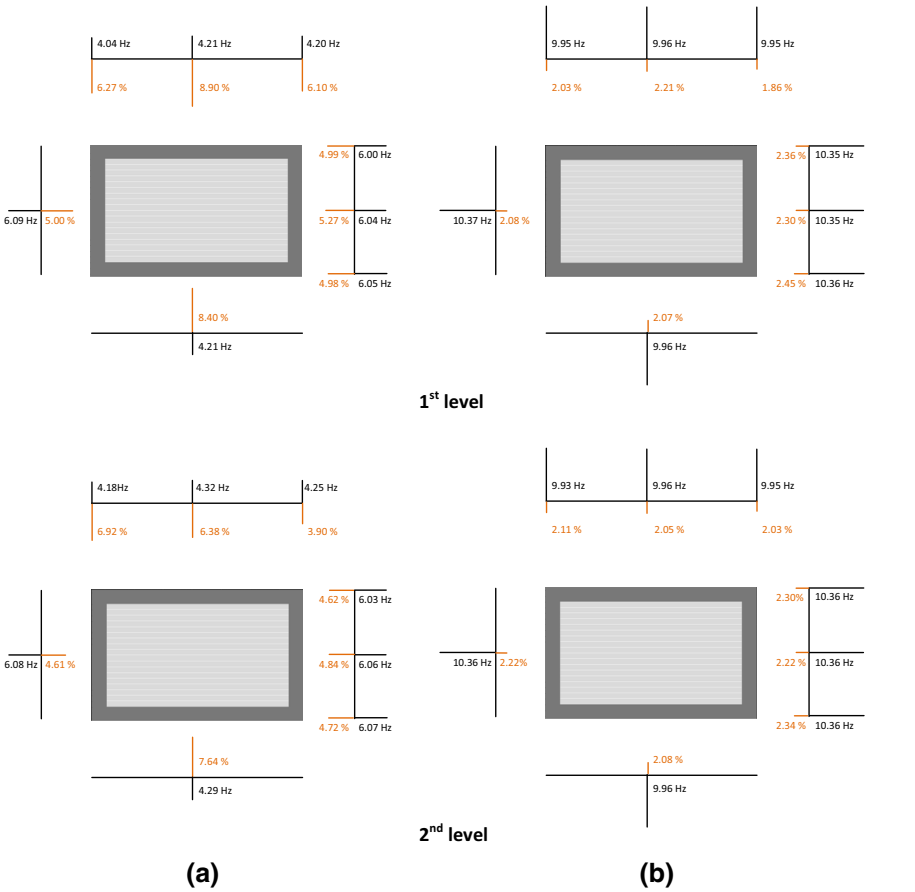

Fig. 12 PBM. Resonance frequencies and damping along X and Y axes. **a** PBM-BS and **b** PBM-AS

Table 6 PBM. Dynamic properties

Model	Frequency (Hz)		Damping (%)	
	X	Y	X	Y
PBM-BS	6.05	4.21	4.89	6.81
PBM-AS	10.36	9.95	2.28	2.06

the as built model, along both directions. The features discussed in connection with Fig. 12 and Table 6 are also illustrated in Fig. 13, in which the modal shapes (along X and Y directions) of PBM-BS and PBM-AS models are shown.

Figures 14 and 15 present the variation of the effective frequency and the effective damping of PBM-AS throughout testing (namely, from sine sweep test-1AS to the final test 17AS). By comparing the diagrams along the two directions, one may observe that Kalamata earthquake has affected Y-direction, whereas Irpinia earthquake caused damages in X-direction of the model. Actually, as the imposed base acceleration progressively increased along X direction, the values of frequencies remained constant during Kalamata

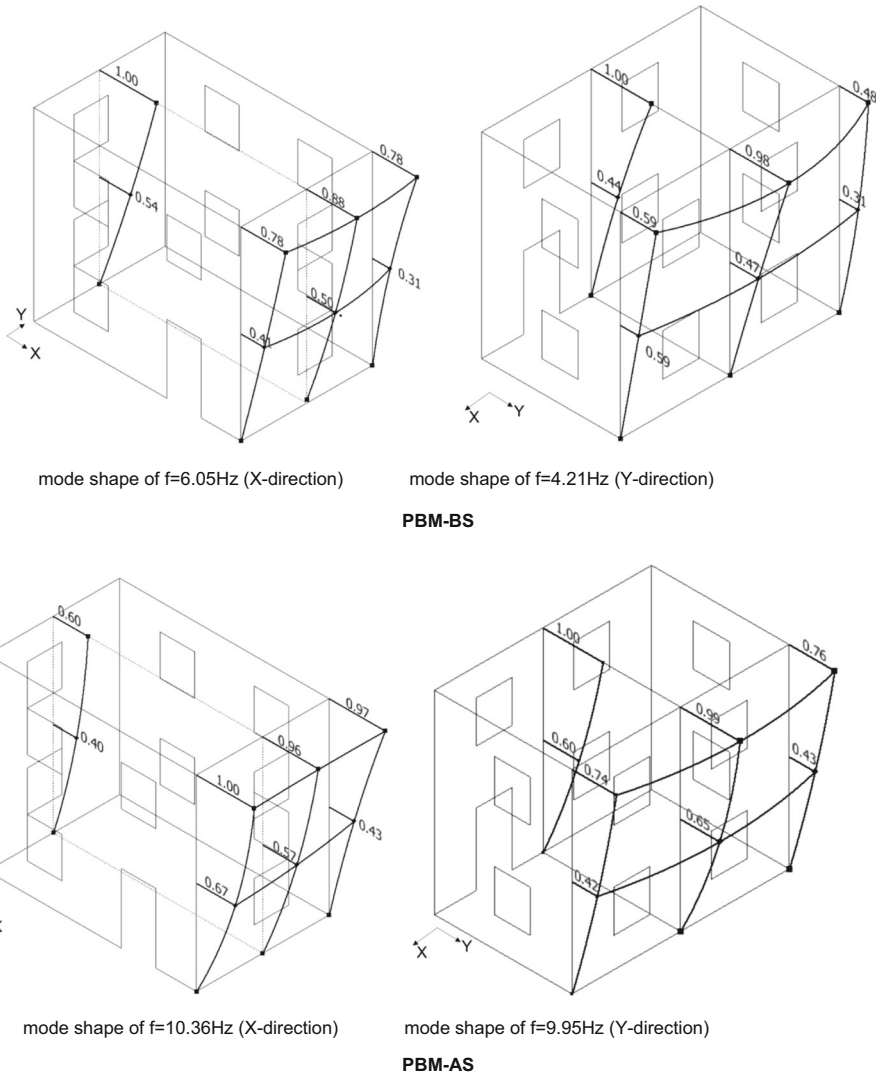

Fig. 13 PBM. Normal mode shapes of the as built and of the strengthened model

earthquake (Fig. 14a), whereas damping exhibited a slight increase (Fig. 14b). This behaviour seems to be in accordance with the observation that the formation of visible damages occurred only during Test 15AS (see following Sect. 3.2). Actually, during the last excitations, significant reduction of frequencies, along with increase of the damping were recorded. Looking at the history of the same properties along the Y-direction, one may observe that the Kalamata earthquake had a significant effect on the model. Actually, after Test 7AS, a decrease of the effective frequency coupled with an increase of damping was recorded (Fig. 15). Under excitations simulating the Irpinia earthquake, higher frequencies were recorded, due to the fact that amplitude of the Irpinia earthquake is lower than that of the Kalamata earthquake.

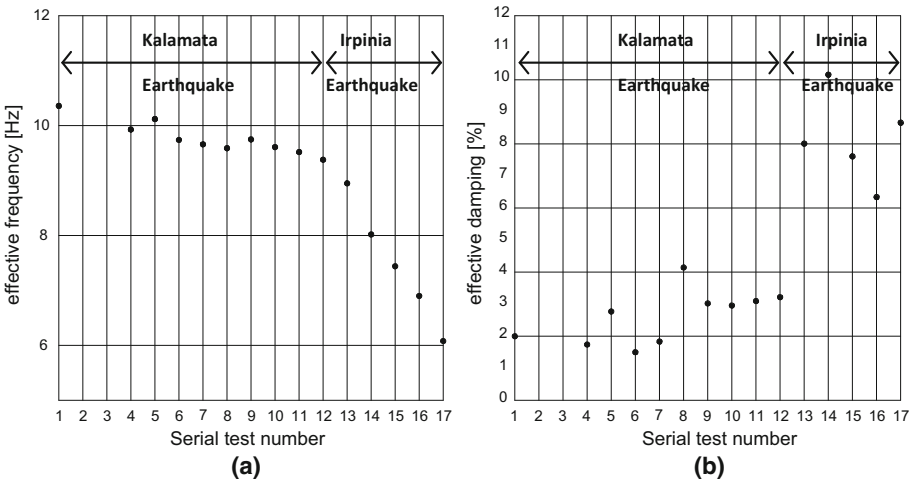

Fig. 14 PBM-AS building. **a** Frequency and **b** damping along X direction during the sequence of shaking table tests [from Test 1AS (Sine sweep test along X direction, Table 5) to Test 17AS (Irpinia earthquake: 0.62 g/0.72 g, Table 5)]

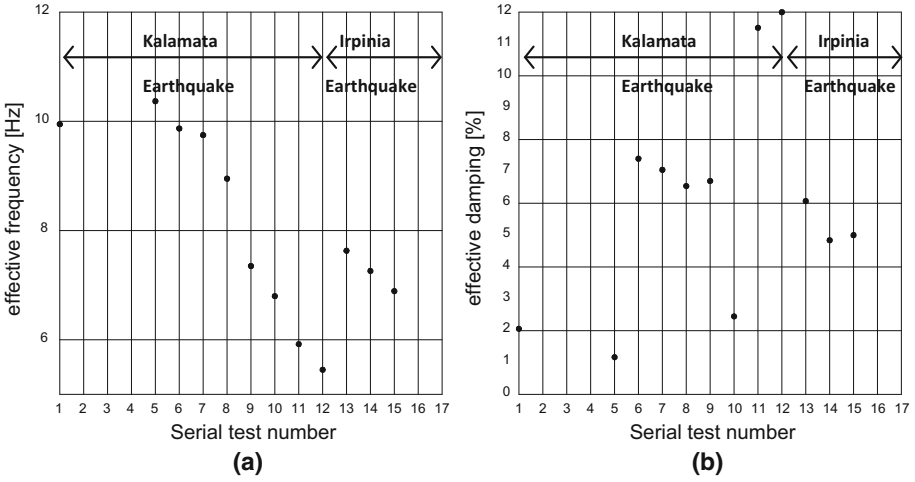

Fig. 15 PBM-AS building. **a** Frequency and **b** damping along Y direction during the sequence of shaking table tests [from Test 2AS (Sine sweep test along Y direction, Table 5) to Test 17AS (Irpinia earthquake: 0.62 g/0.72 g, Table 5)]

3.2 Observed damages

Figures 16 and 17 show the crack pattern of the model before and after its repair and strengthening. The damages shown in the two Figures were surveyed after the completion of the series of tests of PBM-BS and PBM-AS, i.e. after completion of Test 8BS (Kalamata earthquake: 0.29 g(X)/0.24 g(Y)) and Test 17AS (Irpinia earthquake: 0.54 g(X)/0.66 g(Y)) for the as-built and the strengthened model respectively.

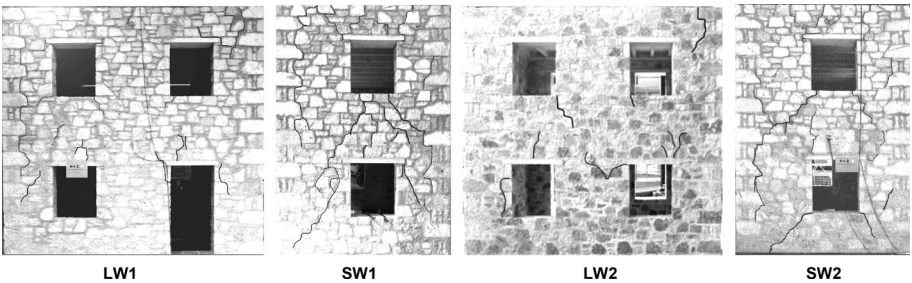

Fig. 16 PBM-As built specimen (BS). Observed damages after Test 8BS (Kalamata earthquake: 0.29 g(X)/0.24 g(Y), Table 4)

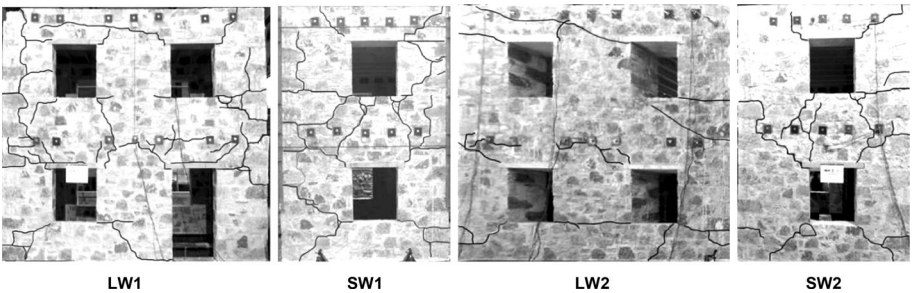

Fig. 17 PBM-Strengthened specimen (AS). Observed damages after Test 17AS (Irpinia earthquake: 0.54 g(X)/0.66 g(Y), Table 5)

In the as-built model (Fig. 16), the short and the long walls exhibited quite different crack patterns. Actually, the short walls, with smaller aspect ratio than the long ones, were more vulnerable in in-plane shear. Shear cracks were formed at both faces of the short walls. However, due to the insufficient diaphragm action of the floors, vertical cracks (due to out-of-plane bending) were also recorded close to the corners of the model, as well as at mid-length of the short walls close to their top. Expectedly, the opening of those cracks decreases from the top to the base of the building. After Test8BS (Kalamata earthquake: 0.29 g(X)/0.24 g(Y), Table 4), the crack width at the top of the model is approximately equal to 8 mm. It is reduced to 6.5–7.0 mm at the level of the lintels, whereas it measures approximately 5.0 mm at the bottom of the window. The long walls of the model are characterized by out-of-plane flexural behaviour. Although some shear cracks have opened at the corners of the openings (Fig. 16), the main cracks are the vertical ones, close to the corners of the building model, separating the long from the short walls.

The tests on the as-built model have proven the vulnerability of the three-leaf masonry. Actually, extensive detachment of the leaves was apparent at all elements of the as-built model (Fig. 18). This separation, initiated in the long walls (at PGA = 0.16 g), was more pronounced close to the corners of the building. Separation was visible also in the regions of openings. It should be reminded here, that (a) there were no header stones connecting the outer leaves of masonry and (b) the additional vertical loads (self weight of the floors and additional masses) were imposed mainly to the inner leaf of masonry. Therefore, pronounced out-of-plane vulnerability of the exterior leaf of masonry was to be expected.

The strengthened model exhibited a significantly improved behaviour, thanks to the better bond between masonry leaves (due to grouting) and, mainly, due to the enhancement of the diaphragm action of the floors and their connection with the perimeter walls. Actually, (a) the model was free of damages after the completion of Test12AS (Kalamata earthquake: 0.55 g(X)/0.39 g(Y), Table 5), (b) no separation between the leaves of masonry was observed, even after the application of the strongest motion (Tests 16AS and 17AS, Table 5), and (c) the vulnerability to out-of-plane bending was significantly reduced. Although vertical cracks (due to out-of-plane bending) were recorded close to failure (Fig. 17), the major failure mechanism of the model is characterized by in-plane bending (under the Irpinia earthquake). As the base acceleration increased to 0.62 g(X)/0.72 g(Y) of Irpinia earthquake (Test 16AS, Table 5), combined rocking and sliding mechanisms were formed and large deformations occurred, without significant force-response degradation though. In Fig. 19, the rigid bodies formed during the repetition of the maximum seismic excitation are shown (thick lines). The building proved to be relatively resilient to earthquake excitation, although extensive cracking occurred. During repetition of the same seismic input (Test 17AS, Table 5), cracking was generalized. Moreover, the cracks that were initially formed at the corners of the openings extended towards the floors, leading to the formation of horizontal cracks at the level of the stiffened diaphragms.

3.2.1 Absolute maximum accelerations recorded on the model at the as-built and at the strengthened state

The sequence of excitations imposed to PBM-BS is shown in Table 4. The recorded accelerations were progressively increasing, up to PGA values of 0.29 g (X)/0.24 g (Y). The sequence of excitations imposed to PBM-AS is shown in Table 5. Both Kalamata and Irpinia earthquake signals were used in this case for the shaking table tests. Again, the accelerations were increased stepwise, up to 0.55 g (X)/0.39 g (Y) of Kalamata earthquake and up to 0.62 g(X)/0.72 g(Y) of Irpinia earthquake. Figure 20 shows the values of the maximum accelerations recorded along the top floor in X and Y directions, both for PBM-BS and PBM-AS. The accelerations shown in Fig. 20 were recorded during the maximum imposed excitation, namely, for PBM-BS Test 8BS (Kalamata earthquake: 0.29 g(X)/0.24 g(Y), Table 4) and for PMB-AS, Test 16AS (Irpinia earthquake: 0.62 g(X)/0.72 g(Y),

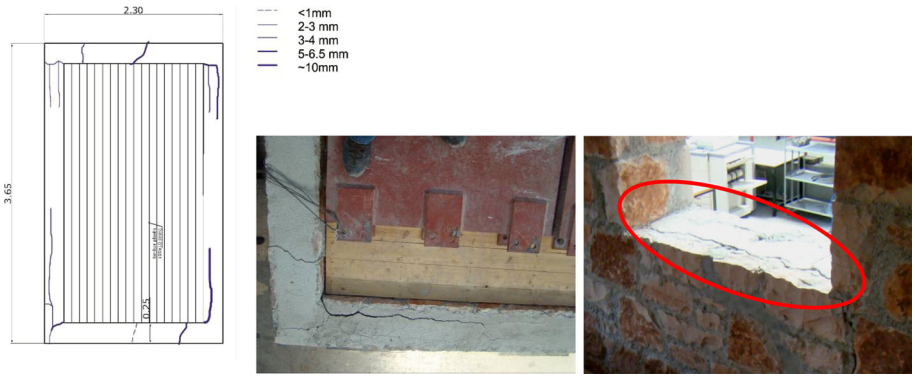

Fig. 18 PBM-As built specimen (BS). Observed damages at the roof level and at the level of openings after Test 8BS (Kalamata earthquake: 0.29 g(X)/0.24 g(Y), Table 4)

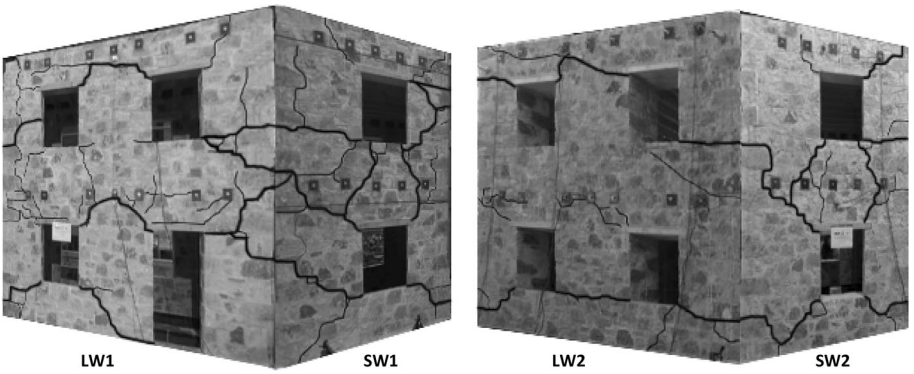

Fig. 19 PBM-Strengthened specimen (AS). Rigid bodies formed during Test 17AS (Irpinia earthquake: 0.54 g(X)/0.66 g(Y), Table 5)

Table 5). The respective maximum recorded accelerations were approximately equal to 0.50 g for PMB-BS and almost 1.00 g for PMB-AS. One may observe the efficiency of the strengthening measures applied to the building model, in terms of maximum acceleration that the strengthened model was able to sustain.

3.3 Relative displacements

Figure 21 presents the maximum relative displacement measured along X and Y directions of the as build model during the excitation that caused damage (Test 6BS: 0.18 g(X)/0.16 g(Y)), as well as during the maximum imposed excitation (Test 8BS: 0.29 g(X)/0.24 g(Y), Table 4). The relative displacements were calculated from the absolute measured displacements at each measuring point, after deduction of the absolute displacement of the base of the model. Displacement values were recorded at mid-length of the walls at both levels of the specimen. One may observe that, for both shaking table tests, the relative displacement was significantly larger for the long walls, as compared to those measured at

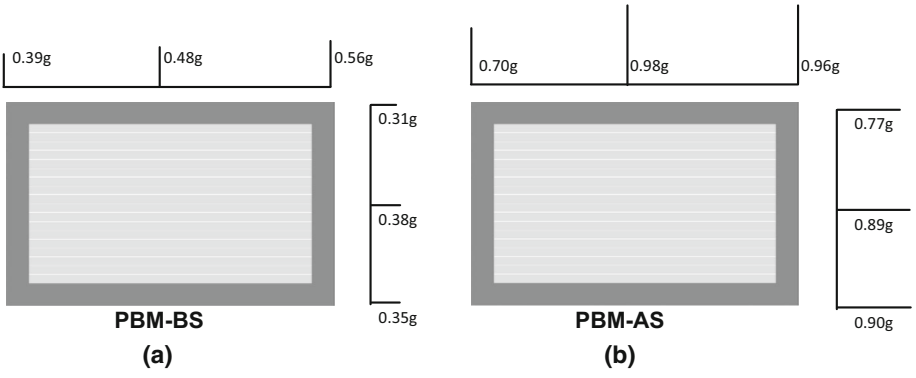

Fig. 20 Maximum accelerations recorded under the maximum imposed excitation along the top floor in X and Y direction **a** of the as built specimen (Test 8BS, Kalamata earthquake: 0.29 g(X)/0.24 g(Y), Table 4) and **b** of the strengthened specimen (Test 16AS, Irpinia earthquake: 0.62 g(X)/0.72 g(Y), Table 5)

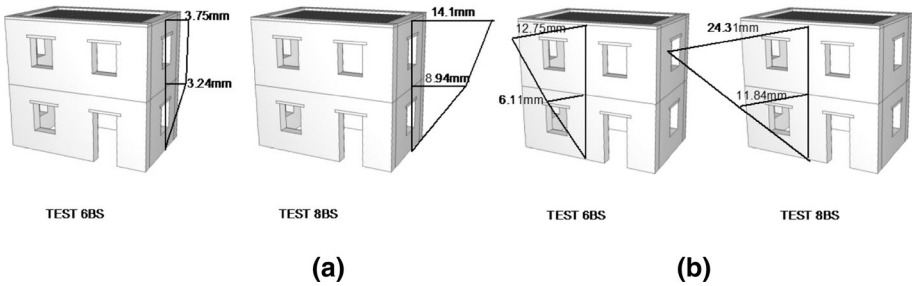

Fig. 21 PBM-As built specimen (BS). Maximum relative displacement along **a** X and **b** Y direction of the as built model recorded during Test 6BS (Kalamata earthquake 0.18 g(X)/0.16 g(Y), Table 4) and Test 8BS (Kalamata earthquake: 0.29 g/0.24 g, Table 4)

the top floor of the short walls. Thus, the pronounced vulnerability of the long walls to out-of-plane bending is confirmed.

Although a direct comparison between the behaviour of PBM-BS and PBM-AS is not considered to be accurate, since the dynamic properties and the stiffness of the strengthened model are modified due to the interventions, it is evident that after strengthening (AS), the relative maximum displacements [recorded for the same seismic input of Kalamata earthquake of 0.29 g(X)/0.24 g(Y)] are significantly reduced (compare Fig. 21: Test 8BS and Fig. 22: Test 8AS).

Relative displacements calculated for PBM-AS as well, for Test 15AS (Irpinia earthquake: 0.48 g(X)/0.43 g(Y), Table 5) and for Test 16AS (Irpinia earthquake: 0.62 g(X)/

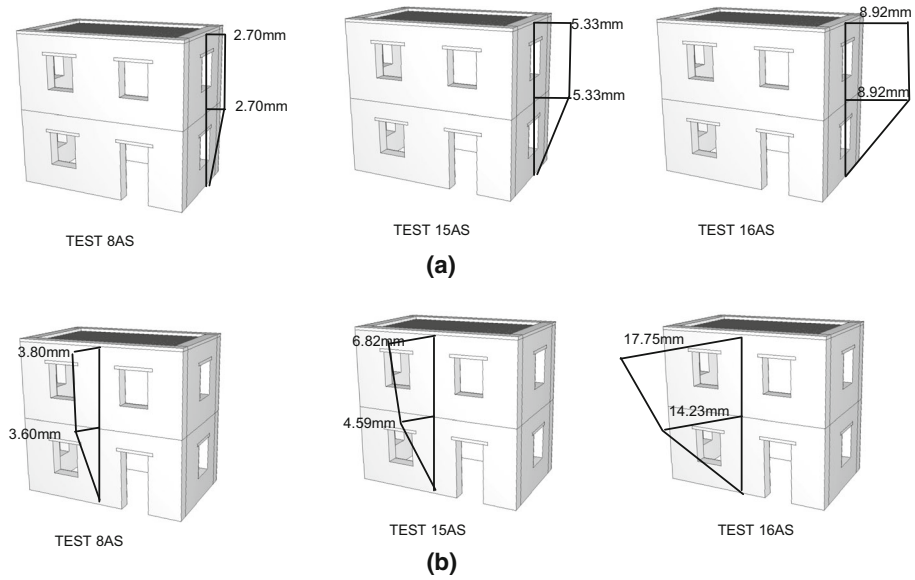

Fig. 22 PBM-AS building. Maximum displacement along **a** X and **b** Y direction of the strengthened model recorded during Test 8AS (Kalamata earthquake: 0.29 g(X)/0.25 g(Y), Table 5) Test 15AS (Irpinia earthquake: 0.48 g(X)/0.43 g(Y), Table 5) and Test 16AS (Irpinia earthquake: 0.62 g(X)/0.72 g(Y), Table 5)

0.72 g(Y), Table 5) are presented in Fig. 22. It is noted that the displacements measured at the top floor for the AS building during Test 16AS (Irpinia earthquake 0.62 g(X)/0.72 g(Y), Table 5) are smaller than those recorded for BS specimen during Test 8BS (Kalamata earthquake: 0.29 g(X)/0.24 g(Y), Table 4). Thus, further evidence on the positive effect of the applied interventions to the box action of the model is provided.

Figure 23 shows the recorded displacements along X and Y direction of the as-built and the strengthened specimen. The large displacements recorded at the corners of the models are attributed to the formation of vertical cracks and the pronounced detachment of the masonry leaves at the wall connections.

The efficiency of the connection between diaphragms and vertical elements was checked during testing of PBM-AS, by measuring the relative floor to wall displacement (Fig. 8). The results of those measurements are plotted in Fig. 24 for Tests 13AS–17AS: It seems that for Test 13AS there is no slip between the floor and the walls, whereas a rather limited residual deformation (of the order of 0.2 mm along both directions) was recorded at the top-floor to wall connection, after the completion of the maximum excitation (Test 16AS, Irpinia earthquake: 0.62 g(X)/0.72 g(Y), Table 5). During the final shaking table test, which is the repetition of Test16AS (Test 17AS, Irpinia earthquake: 0.54 g(X)/0.66 g(Y), Table 5), the model is severely damaged (as described in Sect. 3.2) and the floor-to-wall connections are unable to prevent relative displacements between horizontal and vertical elements.

3.4 Interstorey drift

Interstorey drift values, δ, for both storeys of the building model were calculated for the biaxial excitation that caused damage to the specimen. Those calculations, done both for the PBM-BS and the PBM-AS, were based on measurements taken by displacement transducers D11, D12, D5, D7, D6, D8 (X-direnction) and D9, D10, D1, D3, D2, D4 (Y-direction). The interstorey drift values are presented in Tables 7 and 8.

The results presented in Tables 7 and 8 allow for the following observations to be made: (a) In PBM-BS, the interstorey drifts calculated at mid-length of the long walls are significantly higher than those calculated at mid-length of the short walls. This is attributed to

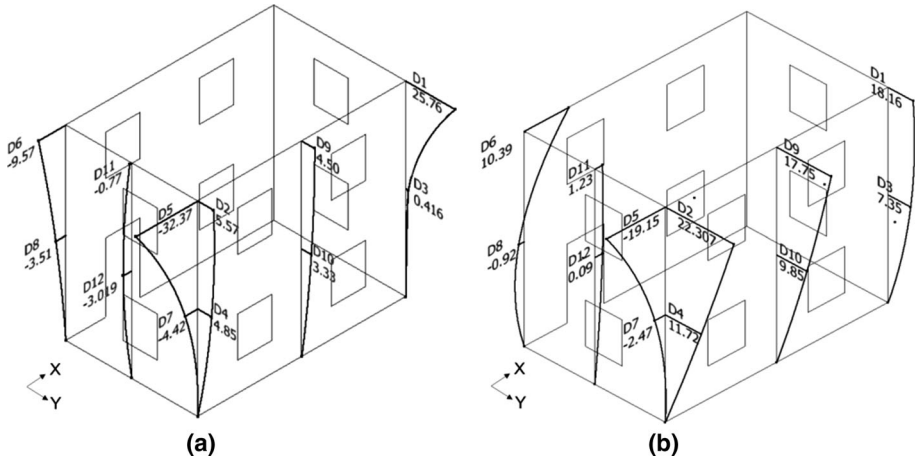

Fig. 23 Displacements along X and Y direction for the **a** unstrengthened model recorded during Test 8BS (Kalamata earthquake: 0.29 g(X)/0.25 g(Y), Table 4) and **b** strengthened model recorded during Test 16AS (Irpinia earthquake: 0.62 g(X)/0.72 g(Y), Table 5)

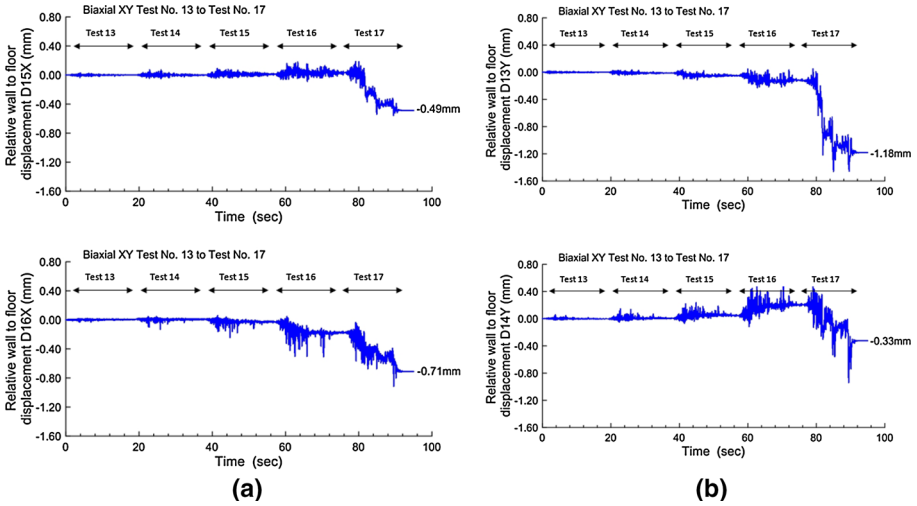

Fig. 24 PBM-AS building. Relative wall to floor displacement along **a** X and **b** Y direction during Tests 13AS (Irpinia earthquake: 0.16 g(X)/0.16 g(Y), Table 5) to Test 17AS (Irpinia earthquake: 0.62 g(X)/0.72 g(Y), Table 5)

the vulnerability of the long walls to out-of-plane bending. On the other hand, (b) Interstorey drift values calculated for the upper floor close to the corner of the model are significantly larger than those calculated at mid-length of the walls. This is in accordance with the observed crack pattern (Sect. 3.2; Figs. 17, 18) that involves large vertical cracks close to the corners of the model, as well as extensive separation between the leaves of masonry. Furthermore, the comparison of the data of Tables 7 and 8, (c) prove the efficiency of the interventions applied to the building model. Actually, the PBM-AS was cracked under an excitation significantly stronger (in terms of maximum imposed acceleration: 0.48 g(X)/0.43 g(Y) vs. 0.18 g(X)/0.16 g(Y)) than the excitation that has caused cracks to the PBM-BS. Moreover, (d) the interstorey drifts at mid-length of long walls are almost equal to those at mid-length of the short walls. Therefore, the enhancement of diaphragm action of floors, combined with efficient connection between floors and walls has led to significant improvement of the box action of the building model, reducing the vulnerability of the long walls to out-of-plane actions. It should be noted that the large value of interstorey drift (30 ‰, Table 8) is attributed to local damage occurred at the location of some measuring devices. Finally, it should be noted that the calculated δ-values are within the limits reported in the literature [summarized in Tomazevic (2010)].

Table 7 PBM-BS. Interstorey drift values at the initiation of cracking (‰)

Floor level	BS-Model, Kalamata earthquake (Test 6BS, 0.18 g(X)/0.16 g(Y))			
	X measurement points D11, D12 (mid-length of short walls)	Y measurement points D9, D10 (mid-length of long walls)	X measurement points D5, D7, D6, D8 (corners of short walls)	Y measurement points D1, D3, D2, D4 (corners of long walls)
1st level	2.03	3.82	4.34	4.62
2nd level	1.70	4.46	11.15	5.13

Table 8 PBM-AS. Interstorey drift values at the initiation of cracking (‰)

Floor level	AS-Model, Irpinia earthquake (Test 15AS, 0.48 g(X)/0.43 g(Y))			
	X measurement points D11, D12 (mid-length of short walls)	Y measurement points D9, D10 (mid-length of long walls)	X measurement points D5, D7, D6, D8 (corners of short walls)	Y measurement points D1, D3, D2, D4 (corners of long walls)
1st level	3.33	2.87	3.14	4.46
2nd level	2.06	2.04	(30.00)	4.42

3.5 Hysteretic response

The hysteretic behaviour of the building model is described through diagrams (Figs. 25, 26, 27, 28) in which absolute acceleration values are plotted against top relative displacement. The hysteretic curves were produced using the recorded measurements of accelerometers A4, A5 and displacement transducers D11, D9 (see Fig. 8) for absolute acceleration and relative displacement in X and Y direction respectively.

Thereby, in Figs. 25 and 26 hysteresis loops are given for longitudinal (X) and transversal (Y) direction respectively [for the Tests 4BS to 8BS (Table 4), i.e. after the occurrence of damage]. One may observe, (a) the significantly smaller stiffness of the system along Y direction, attributed to the out-of-plane behaviour of the long walls, (b) the larger displacements of the model along its weak Y direction and (c) the gradual decrease of the stiffness (along both directions), after the occurrence of damage and under increasing imposed excitations.

Similarly, Figs. 27 and 28 show the hysteresis loops for the strengthened model (for Tests13AS–17AS, Table 5, i.e. after the occurrence of damages). By comparing the two conditions (before and after strengthening), one may observe that (a) strengthening of the building model has led to significant improvement of its behaviour in terms of maximum sustained acceleration. Furthermore, (b) the stiffness of the strengthened model is significantly higher than that of the as-built model. Thus, the deformations sustained by the

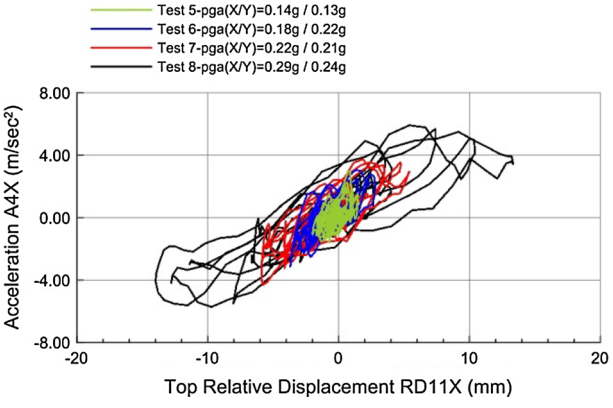

Fig. 25 PBM-As built specimen (BS). Absolute acceleration versus top relative displacement along X direction for Kalamata base motion

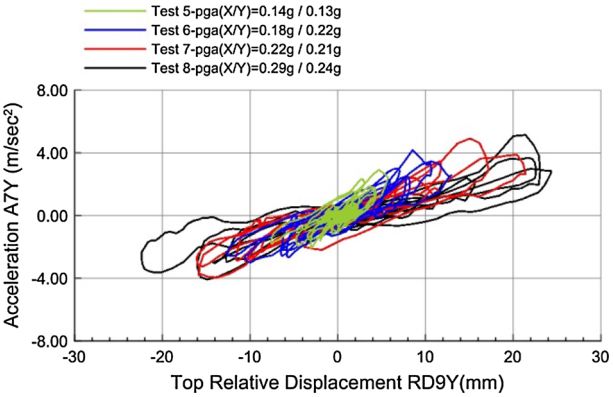

Fig. 26 PBM-As built specimen (BS). Absolute acceleration versus top relative displacement along Y direction for Kalamata base motion

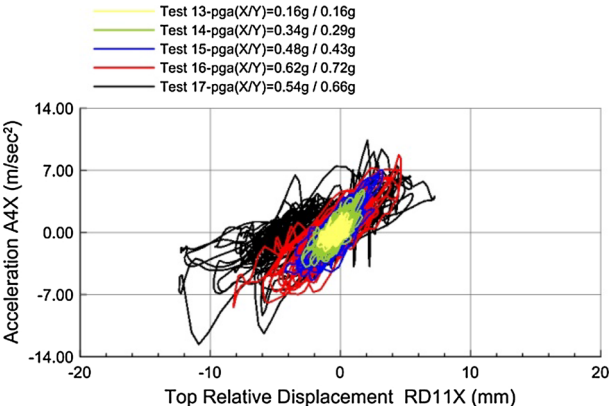

Fig. 27 PBM-Strengthened specimen (AS). Absolute acceleration versus top relative displacement along X direction for Irpinia base motion

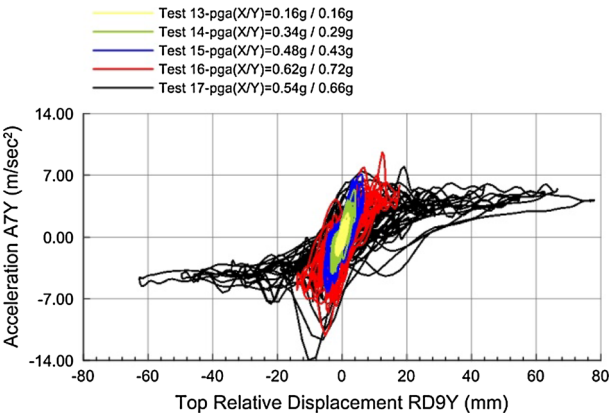

Fig. 28 PBM-Strengthened specimen (AS). Absolute acceleration versus top relative displacement along Y direction for Irpinia base motion

PBM-AS are smaller than those of the PBM-BS even for much higher imposed excitations, (c) Although the box action of the strengthened model is evident, there is still a difference in the displacements imposed along X and Y directions. The formation of a failure mechanism during the final shaking table test (Test17AS), involving rocking and sliding between rigid bodies (compare Fig. 19) can offer an explanation for the increase of measured displacements in Fig. 28.

4 Conclusions

The paper presents the results obtained from shaking table tests on a two storey plain three-leaf stone masonry building model at the as-built state, as well as after damage and strengthening. The purpose of this work was to study the seismic behaviour of typical historic masonry buildings, as well as the effect of widely applied intervention techniques. The experimental results have proven (a) the pronounced vulnerability of three-leaf stone masonry to seismic excitations, as well as (b) the negative effect of flexible wooden floors on the seismic behaviour of historic buildings. Actually, the limited box action of such buildings leads to the occurrence of severe damages due to out-of-plane actions.

On the other hand, the selected scheme of interventions-acceptable also for structures of high architectural value-was very efficient and it rendered the model able to sustain strong input motions. Injecting into masonry a (physico-chemically compatible with in situ materials) hydraulic lime based grout has prevented separation of the leaves of masonry, thus enhancing its out-of-plane stiffness, as well as its mechanical properties. Furthermore, the enhancement of the diaphragm action of floors (by means of a second planking), as well as the improvement of connection between horizontal and vertical elements, led to a building acting as a box. Thus, the deformations of the building model due to the same seismic input were significantly reduced, whereas the strengthened model was able to sustain significantly stronger excitations before cracking and before failure. More specifically, on the basis of the results of the experimental work presented in this paper, the following conclusions may be drawn:

1. For the as-built model, failure is due to shear cracking and, subsequent shear sliding along bed joints for the short walls and to out-of-plane bending for the long walls.
2. Seismic excitations led to early detachment of the leaves of masonry; three-leaf masonry was not provided with header stones, as it is the case in real structures. The separation makes the leaves of masonry vibrate out of phase.
3. The model, after its strengthening, failed due to in-plane bending and rocking of the walls at a significantly higher level of excitation as compared to the as-built model. The response of the walls under rocking is controlled by the strength and stiffness of the diaphragm, which keeps them connected as a whole.
4. Grouting ensured the contact between the three leaves and thus, the bonded leaves behave as monolithic section.
5. Moreover, the strengthened structure exhibited higher stiffness than the unstrengthened one (despite the-moderate though-increase of the mass of the building model due to strengthening). On the contrary, the damping ratio was decreased as a result of the interventions. It is interesting to note that the stepwise increase of the imposed acceleration has led to increased damping ratio without dramatic alteration of the overall stiffness of the building model.

Finally, it should be noted that a direct extrapolation of the experimental results to the behavior of the prototype building is not possible. A detailed analytical work is being carried out, comprising detailed modeling of the 1:2-scaled bulding and validation of the numerical model on the basis of the experimental results. Subsequently, the behaviour of the 1:1 scale building is studied. The results of the numerical calculations performed to date seem to be quite satisfactory.

Acknowledgments This research was funded by the EU FP7-ENV-2009-1, Contract No. 244123 (website: http://www.niker.eu/).

References

Adami C-E, Vintzileou E, Mouzakis C, Badogiannis E, Kalagri A (2012) The effect of hydraulic lime pozzolanic grouts on the mechanical properties of three-leaf stone masonry in compression. In: Proceedings of the 8th international conference on structural analysis of historical construction. Wroclaw, Poland

ASCE 41-06 (2007) Seismic rehabilitation of existing buildings. American Society of Civil Engineers, Reston

Badogiannis E, Miltiadou A, Kalagri A, Ipsilanti E, Dedeloudis C, Vintzileou E (2012) Mix design and performance evaluation of grouts with superfine natural pozzolan. In: Proceedings of 8th international conference SAHC 2012 (Structural Analysis of Historical Constructions). Wrocław, Poland, pp 773–780

Benedetti D, Carydis P, Pezzoli P (1998) Shaking table tests on 24 simple masonry buildings. Earthq Eng Struct Dyn 27(1):67–90

Binda L, Baronio G, Tiraboschi C (1993) Repair of brick-masonries by injection of grouts: experimental Research". J Struct Eng 20(1):29–44

EN1052-1-1998 Methods of test for masonry—part 1: determination of compressive strength

EN 338-2003 Structural timber—strength classes

EN196:1:1994 Methods of testing cement—part 1: determination of strength

European Research Programme NIKER: new integrated knowledge-based approaches to the protection of cultural heritage from earthquake-induced risk, EU FP7-ENV-2009-1, Contract No. 244123 (website: www.niker.eu)

FEMA 356 (2000) Prestandard and commentary for the seismic rehabilitation of buildings

Gavrilovic P, Stankovic V, Bojadziev M (1987) Experimental investigation of a model of masonry building on seismic shaking table, VIII congress of structural engineers, YU

Giuffrè A, Carrocci C (1999) Codice di pratica per la Sicurezza e Conservazione del centro storico di Palermo. Laterza, Bari

Giuffrè A, Baggio C, Carocci C (1993) Sicurezza e conservazione dei centri storici. Laterza, Bari

Harris H, Sabnis G (1999) Structural modeling and experimental techniques, 2nd edn. CRC Press, Boca Raton

http://www.eeri.org/site/projects/learning-from-earthquakes

Juhasova E, Sofronieb R, Bairrao R (2008) Stone masonry in historical buildings—Ways to increase their resistance and durability. Eng Struct 30:2194–2205

Magenes G, Penna A, Galasco A (2010) A full-scale shaking table test on a two storey stone masonry building. In: Proceedings of the 14th European conference on earthquake engineering. Ohrid

Magenes G, Penna A, Rota M, Galasco A, Senaldi I (2012a) Shaking table test of a full scale stone masonry building strengthened maintaining flexible floor and roof diaphragms. In: Proceedings of the 8th international conference on structural analysis of historical construction. Wroclaw, Poland

Magenes G, Penna A, Rota M, Galasco A, Senaldi I (2012b) Shaking table test of a full scale stone masonry building with stiffened floor and roof diaphragms. In: Proceedings of the 15th world conference on earthquake engineering, 24–28 September 2012, Lisbon, Portugal

Manoledaki A-A, Drosos V, Anastasopoulos I, Vintzileou E, Gazetas G (2012) Experimental assessment of the seismic response of three-leaf stone masonry walls, with due consideration to soil–structure interaction. In: Proceedings of the 15th world conference on earthquake engineering, 24–28 September 2012, Lisbon, Portugal

Mazzon N (2010) Influence of grout injection on the dynamic behaviour of stone masonry buildings. PhD Thesis, University of Padova

Mazzon N, Valluzzi MR, Aoki T, Garbin E, De Canio G, Ranierei N, Modena C (2009) Shaking table tests on two multi leaf stone masonry buildings. In: Wael W, El-Dakhakhni, Drysdale RG (eds) Proceedings of the 11th Canadian Masonry Symposium, Toronto

Meguro K, Navaratnaraj S, Sakurai K, Numada M (2012) Shaking table tests on ¼ scaled shapeless stone masonry houses with and without retrofit by polypropylene band meshes. In: Proceedings of the 15th world conference on earthquake engineering, 24–28 September 2012, Lisbon, Portugal

Miltiadou-Fezans A, Tassios TP (2012) Fluidity of hydraulic grouts for masonry strengthening. Mater Struct 45(12):1817–1828

Miltiadou-Fezans A, Tassios TP (2013a) Stability of hydraulic grouts for masonry strengthening. Mater Struct 46(10):1631–1652

Miltiadou-Fezans A, Tassios TP (2013b) Penetrability of hydraulic grouts. Mater Struct 46(10):1653–1671

Miltiadou-Fezans A, Papakonstantinou E, Zambas K, Panou A, Frantzikinaki K (2005) Design and application of hydraulic grouts of high injectability for structural restoration of the column drums of the Parthenon Opisthodomos. In: International conference on structural studies, repairs and maintenance of architectural heritage IX

Miltiadou-Fezans A, Vintzileou E, Papadopoulou E, Kalagri A (2006) Mechanical properties of three-leaf stone masonry after grouting. In: Proceedings of the 5th structural analysis of historical constructions. New Delhi, pp 792–798

Oliver S (2010) A design methodology for the assessment and retrofit of flexible diaphragms in unreinforced masonry buildings. SESOC J 23(1):19–49

Shendova V, Rakicevic Z, Krstevska L, Tashkov L, Gavrilovic P (2012) Shaking table testing of models of historic buildings and monuments—IZIIS' experience. In: Role of seismic testing facilities in performance-based earthquake engineering geotechnical, geological, and earthquake engineering, vol 22, pp 221–245

Tomazevic M (2010) Displacement capacity of masonry buildings as a basis for the assessment of behavior factor: an experimental study. Bull Earthq Eng 8(6):1267–1294

Tomaževic M (1992) Seismic rehabilitation of existing masonry buildings: research and practical implications. In: International symposium on earthquake disaster prevention, vol 2. Mexico, 18–21 May 1992, pp 260–276

Tomaževic M, Sheppard P (1982) The strengthening of stone-masonry buildings for revitalization in seismic regions. In: Proceedings of the 7th European conference on earthquake engineering, vol 5. Athens, pp 275–282

Tomaževic M, Lutman M, Velechovsky T (1993) Aseismic strengthening of old stone-masonry buildings: is the replacement of wooden floors with R.C. slabs always necessary? Eur Earthq Eng 2:34–46

Toumbakari E-E (2002) Lime-pozzolan-cement grouts and their structural effects on composite masonry walls. Doctor Thesis, KU Leuven

Toumbakari E-E, Van Gemert D, Tassios T, Vintzileou E (2003) Effect of the mechanical properties of injection grouts on the structural behaviour of three leaf masonry walls. In: Proceedings of the 9th North American Masonry Conference, South Carolina

Valluzzi MR, da Porto F, Modena C (2001) Behavior of multi-leaf stone masonry walls strengthened by different intervention techniques. In: Proceedings of the 3rd international seminar on "Structural Analysis of Historical Constructions". Guimaraes, Portugal, pp 1023–1032

Valluzzi M-R, Garbin E, Dalla Benetta M, Modena C (2010) In-plane strengthening of timber floors for the seismic improvement of masonry building. In: World conference of timber engineering, Italy

Valluzzi MR, Mazzon N, Garbin E, Modena C (2013) Experimental characterization of out-of plane seismic response of strengthened three-leaf masonry walls by shaking table tests. In: Proceedings of dynamic modal identification of strengthened three-leaf stone masonry walls subjected to out-of-plane shaking table tests, 15th ANIDIS Conference, 30th June–4th July, Padova, Italy

Vasconcelos G, Lourenco PB (2009) In-plane experimental behavior of stone masonry walls under cyclic loading. J Struct Eng 135:1269–1277

Vintzileou E (2011) Three-leaf masonry in compression, before and after grouting: a review of literature. International Journal of Architectural Heritage 5(4–5):513–538

Vintzileou E, Tassios T (1995) Three-leaf stone masonry strengthened by injecting cement grout. J Struct Eng 121(5):848–856

Wilson A (2012) Seismic assessment of timber floor diaphragms in unreinforced masonry buildings. Doctor Thesis, University of Auckland